Magnetic record of extreme marine inundation events at Las Salinas site, Jalisco, Mexican Pacific coast

Article *in* International Geology Review · August 2015

DOI: 10.1080/00206814.2015.1075230

CITATIONS
5

READS
269

8 authors, including:

Jan Cerny
Masaryk University
7 PUBLICATIONS **21** CITATIONS
SEE PROFILE

María Teresa Ramírez-Herrera
Universidad Nacional Autónoma de México
76 PUBLICATIONS **595** CITATIONS
SEE PROFILE

María Felicidad Bógalo
Universidad de Burgos
37 PUBLICATIONS **110** CITATIONS
SEE PROFILE

Rocio Castillo-Aja
University of Guadalajara
17 PUBLICATIONS **7** CITATIONS
SEE PROFILE

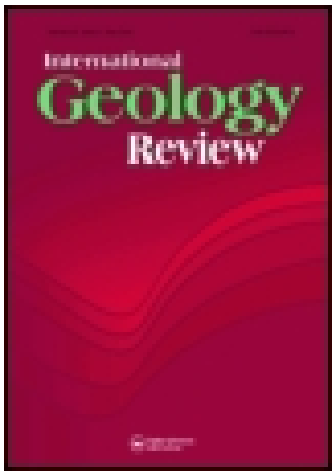

International Geology Review
Publication details, including instructions for authors and subscription information:
http://www.tandfonline.com/loi/tigr20

Magnetic record of extreme marine inundation events at Las Salinas site, Jalisco, Mexican Pacific coast

Jan Černý[ab], María-Teresa Ramírez-Herrera[cd], María-Felicidad Bógalo[e], Avto Goguitchaichvili[f], Rocío Castillo-Aja[g], Juan Morales[f], Joan Albert Sanchez-Cabeza[h] & Ana Carolina Ruiz-Fernández[h]

[a] Department of Geological Sciences, Faculty of Science, Masaryk University, Brno, Czech Republic

[b] Institute of Geology, Academy of Sciences of the Czech Republic, Prague-Lysolaje, Czech Republic

[c] Laboratorio Universitario de Geofisica Ambiental & Departamento de Geografia Fisica, Instituto de Geografia, Universidad Nacional Autonoma de Mexico, Ciudad Universitaria, Mexico City, Mexico

[d] Active Tectonics Group, Berkeley Seismological Laboratory, University of California Berkeley, Berkeley, CA, USA

[e] Departamento de Física, Escuela Politécnica Superior, Universidad de Burgos, Burgos, Spain

[f] Laboratorio Interinstitucional De Magnetismo Natural, Instituto De Geofisica, Universidad Nacional Autónoma De Mexico - Campus Morelia, Michoacán, Mexico

[g] Posgrado en Geografía, Universidad Nacional Autónoma de México, Ciudad Universitaria, Mexico City, Mexico

[h] Instituto de Ciencias del Mar y Limnología, Universidad Nacional Autónoma de México, Ciudad Universitaria, Mexico City, Mexico

Published online: 07 Aug 2015.

To cite this article: Jan Černý, María-Teresa Ramírez-Herrera, María-Felicidad Bógalo, Avto Goguitchaichvili, Rocío Castillo-Aja, Juan Morales, Joan Albert Sanchez-Cabeza & Ana Carolina Ruiz-Fernández (2015): Magnetic record of extreme marine inundation events at Las Salinas site, Jalisco, Mexican Pacific coast, International Geology Review, DOI: 10.1080/00206814.2015.1075230

To link to this article: http://dx.doi.org/10.1080/00206814.2015.1075230

INTERNATIONAL GEOLOGY REVIEW, 2015
http://dx.doi.org/10.1080/00206814.2015.1075230

Taylor & Francis
Taylor & Francis Group

Magnetic record of extreme marine inundation events at Las Salinas site, Jalisco, Mexican Pacific coast

Jan Černý[a,b], María-Teresa Ramírez-Herrera[c,d], María-Felicidad Bógalo[e], Avto Goguitchaichvili[f], Rocío Castillo-Aja[g], Juan Morales[f], Joan Albert Sanchez-Cabeza[h] and Ana Carolina Ruiz-Fernández[h]

[a]Department of Geological Sciences, Faculty of Science, Masaryk University, Brno, Czech Republic; [b]Institute of Geology, Academy of Sciences of the Czech Republic, Prague-Lysolaje, Czech Republic; [c]Laboratorio Universitario de Geofisica Ambiental & Departamento de Geografia Fisica, Instituto de Geografia, Universidad Nacional Autonoma de Mexico, Ciudad Universitaria, Mexico City, Mexico; [d]Active Tectonics Group, Berkeley Seismological Laboratory, University of California Berkeley, Berkeley, CA, USA; [e]Departamento de Física, Escuela Politécnica Superior, Universidad de Burgos, Burgos, Spain; [f]Laboratorio Interinstitucional De Magnetismo Natural, Instituto De Geofisica, Universidad Nacional Autónoma De Mexico - Campus Morelia, Michoacán, Mexico; [g]Posgrado en Geografía, Universidad Nacional Autónoma de México, Ciudad Universitaria, Mexico City, Mexico; [h]Instituto de Ciencias del Mar y Limnología, Universidad Nacional Autónoma de México, Ciudad Universitaria, Mexico City, Mexico

ABSTRACT

Extreme marine inundation events (i.e. severe storms and tsunamis) denote a major hazard to coastal communities around the globe. In order to assess this hazard, long-term (beyond the instrumental and historic records) information on the magnitude and frequency of these events is critical. The coastal sedimentary record, together with other proxies, is now being tested to distinguish and reconstruct evidence of ancient inundation events. Recent studies commonly use anisotropy of magnetic susceptibility (AMS) parameters without statistical evaluation of the lateral variability of sedimentary layers. Here, we provide results from tested sedimentary layers. Moreover, we discuss the most recent strategies to identify deposits produced by major inundation events using the full battery of rock magnetic properties of sediments in Careyes Bay on the Jalisco coast, Eastern Pacific, a tectonically active coast subject to hurricanes. Oriented samples of lagoonal sediments were taken from a dug pit at Las Salinas site. The sampled stratigraphic sequence was basically composed of an upper sand and lower clay units. The upper part of the Las Salinas profile shows a drop in magnetic susceptibility by 50%. Two distinct magnetic fabrics are clearly identified. Fabric from the upper part of the profile most probably reflects a sedimentary structure which was originated in a more dynamic environment than the magnetic fabric recognized in the lower part of the profile. Hysteresis parameters also show variation in behaviour between the upper and lower parts of the profile. We propose here that the origin of the upper sand unit at the study site is most probably related to an extreme marine inundation event.

ARTICLE HISTORY
Received 14 May 2015
Accepted 19 July 2015

KEYWORDS
Anisotropy of magnetic susceptibility (AMS); rock magnetic properties; tsunami; thermomagnetic curves; Mexican Pacific coast; variability

1. Introduction

The magnetic signature of extreme marine inundation deposits emerges as a valuable tool to fully understand these events in the context of the coastal environment. It remains problematic to distinguish whether the sediment laid down by a marine inundation was deposited by either a tsunami or storm event (e.g. Kamatani 1982; Tuttle *et al*. 2004; Kench *et al*. 2006, 2008; Morton *et al*. 2007; Jankaew *et al*. 2008).

Several studies show that not one but a series of diagnostic criteria must be used to reveal the differences between tsunami and storm deposits (e.g. Morton *et al*. 2007; Kortekaas and Dawson 2007; Richmond *et al*. 2011). However, only a few studies used a combination of proxies to match these criteria to try to identify the nature of high-energy marine inundation deposits (Ramírez-Herrera *et al*. 2007, 2012, 2014; Chagué-Goff *et al*. 2011, 2012). The use of multiple proxies is even more important in distinguishing the differences between tsunami deposits and other high-energy inundation events. Studies on marine inundation deposits have begun recently on the Mexican Pacific coast (Ramírez-Herrera *et al*. 2005, 2007, 2009, 2012, 2014).

The study area is situated on the active Mexican continental margin, where both storm and tsunami inundations occur. Whereas storm inundations have a climatic cause, tsunami inundations are related to submarine landslides and/or seismic events. Tsunamigenic earthquakes in the area are related to the active zone where the Cocos

CONTACT: Jan Černý 176111@mail.muni.cz.
Supplemental data for this article can be accessed at http://dx.doi.org/10.1080/00206814.2015.1075230

plate and Rivera microplate subduct beneath the North American plate. Over recent years several studies have dealt with the characteristics of the subduction zone, such as seismicity and tectonics along the Mexican active margin and the potential of this area to produce tsunamigenic earthquakes (e.g. Ramírez-Herrera and Urrutia-Fucugauchi 1999; Núñez-Cornú *et al*. 2002; Ferrari *et al*. 2012; Manea *et al*. 2013); however, several questions remain unanswered. Of particular interest to our study are the events of 3 June 1932 (Ms 8.2) and 9 October 1995 (Mw 8.0) – tsunamigenic earthquakes that hit the study area. The earlier event was described in historical records (Corona and Ramírez-Herrera 2012a, 2012b) while the more recent event was instrumentally recorded (Borerro *et al*. 1997; Ortiz *et al*. 1998).

Magnetic studies have emerged as important tools for the identification of tsunami deposits. Initial attempts to incorporate magnetic studies as proxy in tsunami deposits studies were performed recently (Font *et al*. 2010; Wassmer *et al*. 2010). Since then, magnetic proxies such as magnetic susceptibility (MS) measurements or anisotropy of magnetic susceptibility (AMS) have become an innovative tool used in tsunami deposit studies (e.g. Ramírez-Herrera *et al*. 2012, 2014; Cuven *et al*. 2013; Font *et al*. 2013; Schneider *et al*. 2014). However, the potential of magnetic proxies in marine inundation deposit studies is still under consideration. Therefore providing new magnetic data of inundation deposits in new ways will contribute to improving the usefulness of such studies in order to characterize the internal properties of sediments.

2. Material and methods

Oriented samples of lagoon sediments were collected from a dug pit at Las Salinas marsh, site 004, on the Jalisco coast, Mexico (Figure 1). The coastal stratigraphy at the site consists of four upper sand units while the lower part consists of two clay units. We will refer to these units henceforth as the upper sand and lower clay unit for general comparison to the magnetic properties analysis. The upper sand unit has a sharp basal contact that varies locally in depth. For detailed description, see the stratigraphic profile in Figure 2.

2.1. Magnetic methods

At the locality Las Salinas 004, samples for magnetic studies were collected in two ways: (1) samples for AMS analysis were collected from four individual depth horizons at 7–9, 13–15, 21–23, and 43–45 cm, where eight samples were collected from each depth interval to verify lateral variability (horizontal distance between individual samples was about 3 cm); (2) along a continuous vertical profile every 2 cm, starting from 1 cm below the surface to a depth of 45 cm (22 samples in total). These samples were used for the other detailed rock magnetic measurements and age determination, which are described below. All AMS measurements were conducted at the Institute of Geophysics of the National Autonomous University of Mexico, using the KLY-2 Kappabridge device (applied field of 423 A/m).

The remaining rock magnetic measurements were carried out at the Palaeomagnetic Laboratory of Burgos University (Spain). Low-field MS (x), expressed in $m^3\ kg^{-1}$, was measured using a KLY-4 Kappabridge (AGICO, applied field of 300 A/m and noise level 3×10^{-8} S.I.) and normalized by the mass of the sample. Frequency-dependent susceptibility (x_{fd}) was obtained using a MS2 meter (Bartington, with dual frequency 0.47 and 4.7 kHz) on the basis of the equation $x_{fd} = 100 \times (x_{lf} - x_{hf})/x_{lf}$, where x_{lf} and x_{hf} are the magnetic susceptibilities measured at low and high frequency, respectively. This parameter is commonly used in rock magnetic environmental studies to evaluate the contribution of fine-grained ferrimagnetic particles lying within the superparamagnetic/single-domain (SP/SD) threshold size (Dearing *et al*. 1996). In order to characterize the mineralogy and the magnetic properties of ferromagnetic particles, a variable field translation balance (VFTB) was utilized based on the following measurement sequence: (1) isothermal remanent acquisition curve (IRM or M_r) up to 1 T; (2) hysteresis loop (±1 T); (3) backfield demagnetization curves to measure the coercivity of remanence; and (4) in-field thermomagnetic curve (*M*–*T*). The thermomagnetic experiments were performed in air up to 700°C and cooled to room temperature in an applied field of 38 mT, at a heating and cooling rate of 30°C min^{-1}. Curie temperatures were determined using the two-tangent method (Grommé *et al*. 1969). Hysteresis parameters, such as saturation magnetization (M_s), saturation remanence magnetization (M_{rs} or *SIRM*), and coercive field (B_c), were calculated from hysteresis loops after subtracting the paramagnetic contribution and remanence coercivity (B_{cr}) from backfield curves. These parameters were measured using the RockMagAnalyzer 1.0 sofware (Leonhardt 2006). In addition, six representative samples were submitted to IRM stepwise acquisition experiments up to 2 T using a M2 T-1 pulse magnetizer. IRM acquisition curves were fitted by a linear combination of cumulative log Gaussian functions (GLC), each corresponding to a single magnetizable mineral phase (Robertson and France 1994). The statistical analysis was carried out following Kruiver *et al*. (2001) and Heslop *et al*. (2002). Obtained magnetic components are characterized by three parameters: saturation magnetization (SIRM), mean coercivity ($B_{1/2}$), and dispersion of cumulative log-normal

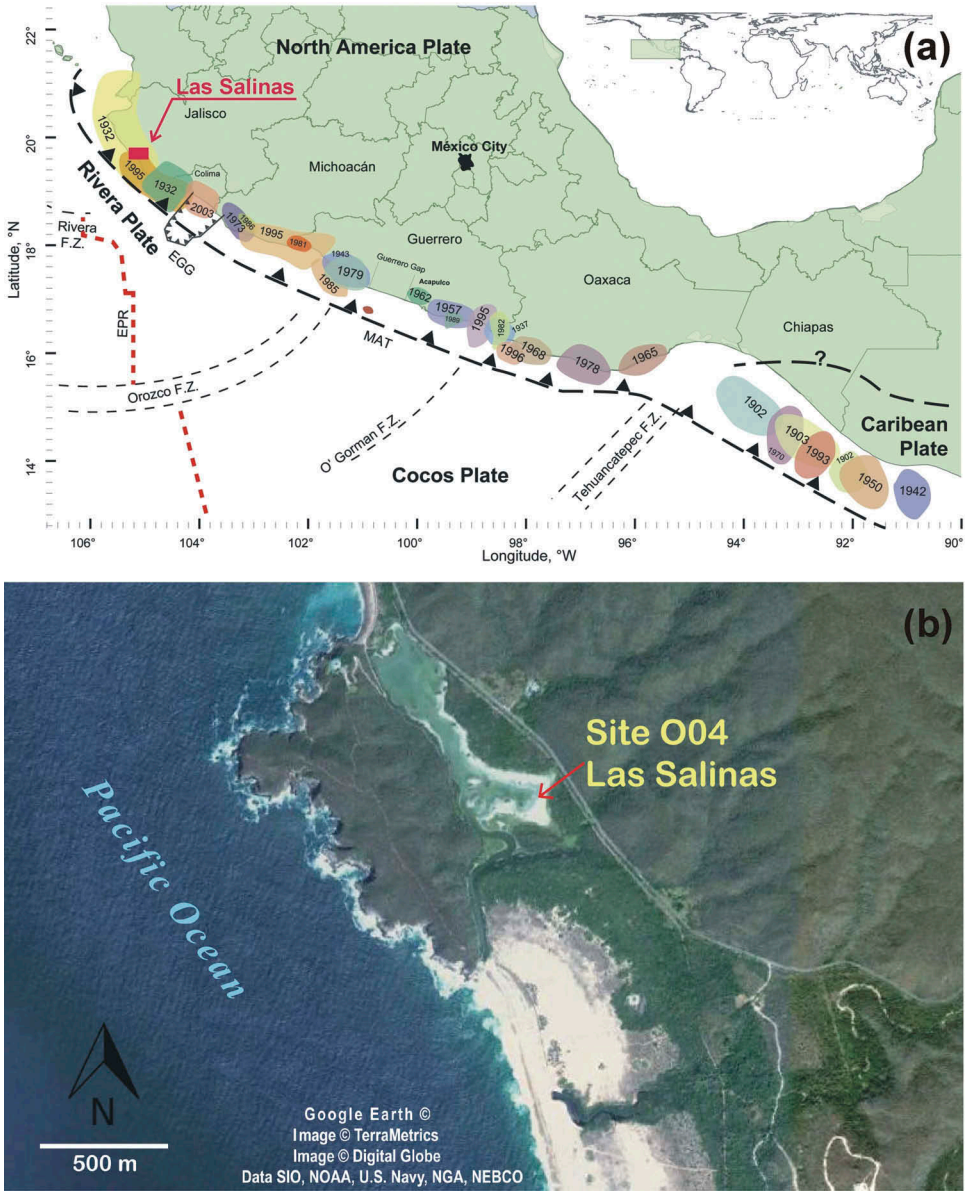

Figure 1. (a) Tectonic and seismic setting of the Pacific coast of Mexico: MAT, Middle American Trench; FZ, fracture zones; EPR, East Pacific rise; EGG, El Gordo Graben. Different-coloured dots indicate rupture areas and years of most important subduction seismic events since the beginning of the last century. Thin black dashed lines indicate fracture zones; the thick black dashed line with arrowheads shows the subduction zone; the thick red dashed line shows the location of the EPR. The boundary between the Caribbean and North American plates is shown by a dashed line and question mark as it is not well defined. The solid red box shows the location of the satellite image below (not to scale); (b) satellite image of the investigated area with marked position of the sampling site 004 Las Salinas.

distribution (DP). Note that the magnetization values were normalized by the mass (unit $Am^2\ kg^{-1}$).

The temperature dependence of MS was determined in both air and argon for selected samples up to 700°C using a CS3 furnace attached to a KLY-4 Kappabridge, at a heating and cooling rate of approximately 11°C min^{-1} and in a field of 300 A/m.

AMS in low field was measured at room temperature using a KLY-2 Kappabridge. Principal susceptibility directions $\mathbf{K_1}$, $\mathbf{K_2}$, and $\mathbf{K_3}$ correspond to maximum, intermediate, and minimum susceptibility directions respectively. Based on these principal directions, the following AMS parameters were calculated: shape parameter, *T* (Jelinek 1981); degree of anisotropy, *P* (Nagata 1961); mean MS, K_m; shape factor, *q* (originally named as the azimuthal anisotropy quotient; Granar 1958); magnetic lineation, *L* (Khan 1962); and magnetic foliation, *F* (Khan 1962). AMS data were analysed using the Anisoft 4.1 software. The correct mathematical typography is used to distinguish between scalars (*italics*) and vectors (**bold**) throughout this paper to avoid misunderstanding.

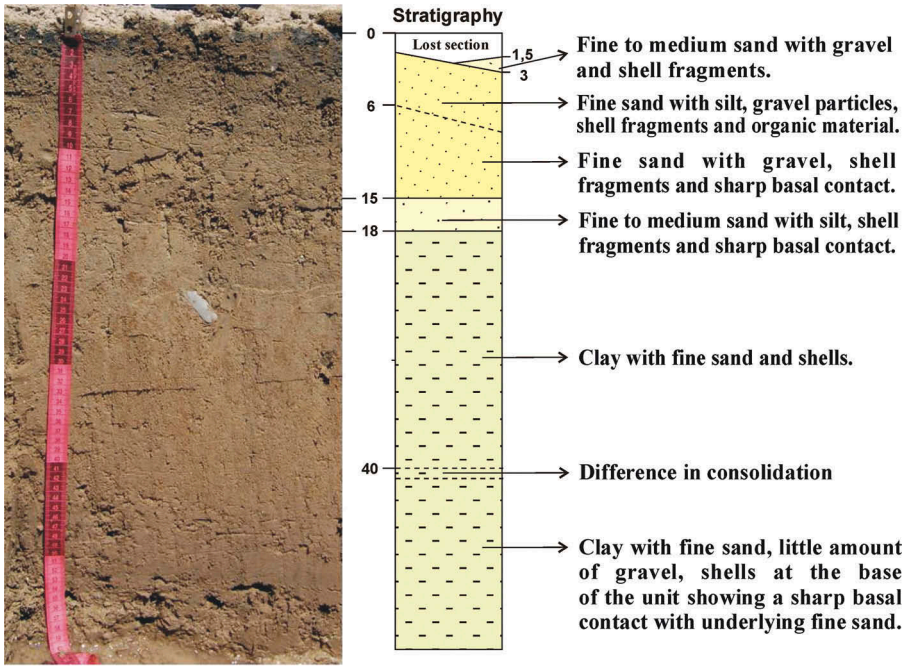

Figure 2. Stratigraphic section at Las Salinas 004 site. Numbers along the profile represent depth in centimetres.

2.2. Radiometric dating

Detailed interpretation of the timing of marine inundation events recorded in the sedimentary record requires accurate dating. The generally accepted way to date sediments deposited over the last 100–150 years is to use ^{210}Pb radionuclide (Krishnaswamy *et al*. 1971; Sanchez-Cabeza and Ruiz-Fernández 2012).

^{210}Pb is a natural radionuclide of the ^{238}U radioactive chain, with a half-life of $t_{½}$ = 22.23 ± 0.12 years; its activity in sediments ($^{210}Pb_{total}$) is the sum of the ^{210}Pb produced *in situ* ($^{210}Pb_{sup}$) from the radioactive disintegration from its parent radionuclide ^{226}Ra ($t_{½}$ = 1600 years), and the ^{210}Pb supplied mostly from the atmosphere (unsupported or excess ^{210}Pb = $^{210}Pb_{xs}$) derived from the decay of ^{222}Rn, which emanates from soils (Sanchez-Cabeza and Ruiz-Fernández 2012). ^{210}Pb dating is based on the $^{210}Pb_{xs}$ activity depth profile, which should show a logarithmically decreasing trend with depth as a result of the radioactive decay over time, according to the radioactive decay law:

$$^{210}Pb_{(z)} = {}^{210}Pb_{(0)}e^{-\lambda t},$$

where $^{210}Pb_{(0)}$ is the surface activity, $^{210}Pb_{(z)}$ is the activity at depth z, and λ is the decay constant (0.03118 year^{-1}). This equation assumes a constant supply of ^{210}Pb and particles to the sediments, as well as a negligible post-depositional migration of ^{210}Pb within the column (Appleby 1998).

^{210}Pb dating is often supported by the marker ^{137}Cs ($t_{½}$ = 30.14 years), since the use of both radiotracers improves accuracy by providing two independent means of measuring the same burial processes occurring within a given sediment core. The artificial radionuclide ^{137}Cs ($t_{½}$ = 30.5 ± 0.8 year) is present in the environment mainly due to fallout from the atmospheric testing of thermonuclear weapons. Significant fallout on a global scale began shortly after the initial testing in the early 1950s, peaked in 1963, and then rapidly declined following implementation of the international treaty banning such tests (DeLaune *et al*. 1978). Therefore, undisturbed sediments around the world are expected to show a ^{137}Cs activity profile in which the first detectable activities correspond to the decade from 1950, the maximum ^{137}Cs activity to the period 1962–1964, and a decreasing trend thereafter.

The activities of ^{210}Pb, ^{226}Ra, and ^{137}Cs were determined in sediment samples of Sal-005 collected in 1 cm steps between the surface and 15 cm depth following the procedure of Sanchez-Cabeza and Ruiz-Fernández (2012).

3. Results

All data were classified by their corresponding lithology into two sets that represent the upper sand unit and the lower clay unit. The upper sand unit was sampled between 1 and 17 cm, whereas the lower clay unit was sampled between 17 and 45 cm depth.

3.1. Thermomagnetic studies

Thermomagnetic curves (*M–T*) were measured for every stratigraphic level. Two slightly different patterns are related to upper and lower units (Figure 3). Samples from the lower unit exhibit the highest magnetization values, with the exception of sample 004–02 (3–5 cm). These samples are characterized by the presence of two phases in the heating curve: magnetite, with a Curie temperature of about 580ºC, and another lower-temperature phase with Curie temperature between 350–380ºC, which could correspond to titanomagnetite, titanohematite, or (titano)maghemite. On the other hand, in the upper unit the Curie temperature values for the high-Curie temperature phase are similar to those calculated in the lower unit. However, the curves show a smooth decay for the low-temperature phase with a Tc around 400ºC, but this is not present in some of them. All samples showed lower magnetization after heating to 700ºC, and only magnetite (mean Tc = 570ºC) is observed.

The temperature dependence of MS was performed on two samples, one each representing the upper and lower units. Slight differences are also visible on the plot in Figure 11(b) (see Section 4). Both curves show an inflection point between 575 and 585°C. Moreover, the lower layer curve shows increasing MS at the beginning, followed by a gradual drop between 270 and 530°C and then a sharp decrease with an inflection point between 575 and 585°C.

3.2. AMS

The magnetic fabric from the upper part of the profile (I, sampled at 7–9 and 13–15 cm horizons) shows subhorizontal $\mathbf{K_1}$ and $\mathbf{K_2}$ mean directions, whereas the mean $\mathbf{K_3}$ is oriented vertically. Fabric I is more scattered in comparison with the results of AMS from the lower part of the profile (II, sampled at 21–23 and 43–45 cm horizons). The mean direction of $\mathbf{K_1}$ in the case of magnetic fabric II is oriented in azimuth 217°, but mean $\mathbf{K_3}$ direction is tilted from the vertical line by about 35° and $\mathbf{K_2}$ by about the same angle from the horizontal plane. The mean MS of samples related to magnetic fabric I (blue and green squares, Figure 4) is lower than the mean MS of samples related to magnetic fabric II (red and yellow squares, Figure 4). Axial confidence cones at the 95% level for the upper and lower units overlap, which makes mean axes $\mathbf{K_2}$ and $\mathbf{K_3}$ of both units barely distinguishable. Nevertheless, the characteristics of these fabrics are different: the deviation of mean axes in the lower unit is much less than in the upper one and the confidence ellipse is more or less isometric, while the $\mathbf{K_2}$ and $\mathbf{K_3}$ confidence ellipses of the fabric I are elongated. The Jelinek *P–T* diagram indicates that the dispersal of the shape parameter, *T*, increases with a decreasing degree of anisotropy, *P* (Figure 4).

Due to observations of variability in the horizontal direction (i.e. across profile), the AMS was measured on samples from four horizons (see Supplementary Material at http://dx.doi.org/10.1080/00206814.2015.1075230 for primary data). The boundaries for maximal and minimal parameter values, as well as their standard deviations, were established separately for each horizon. The range of parameter values is given by horizontal changes in sediment properties (Figure 5).

3.3. MS and hysteresis parameters

Rock magnetic parameters exhibit variation in behaviour depending on the layer involved. Magnetic parameters, such as MS (χ), saturation remanence magnetization (M_{rs}), and saturation magnetization (M_s), show similar variations with depth (Figure 6). At

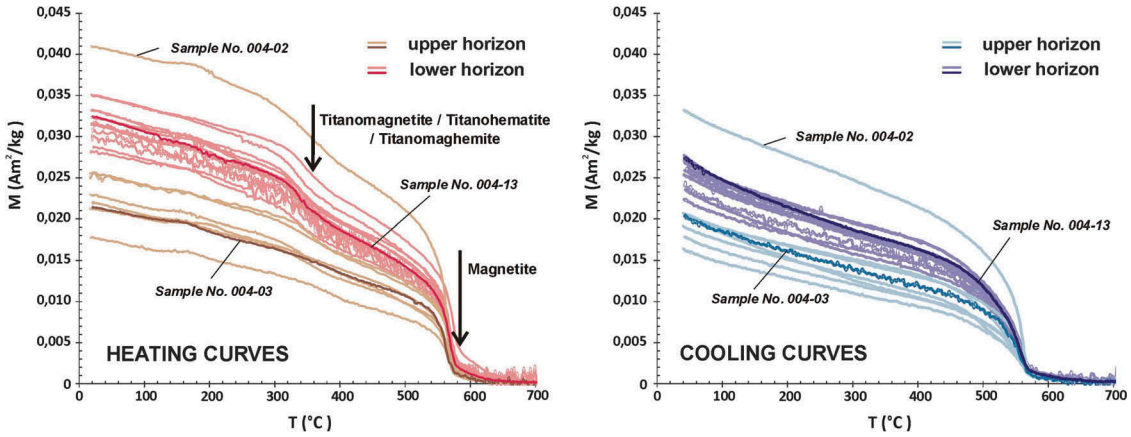

Figure 3. Thermomagnetic curves for all samples along the Las Salinas section. Samples corresponding to the lower layer show higher values of *M* in comparison with those from the upper layer.

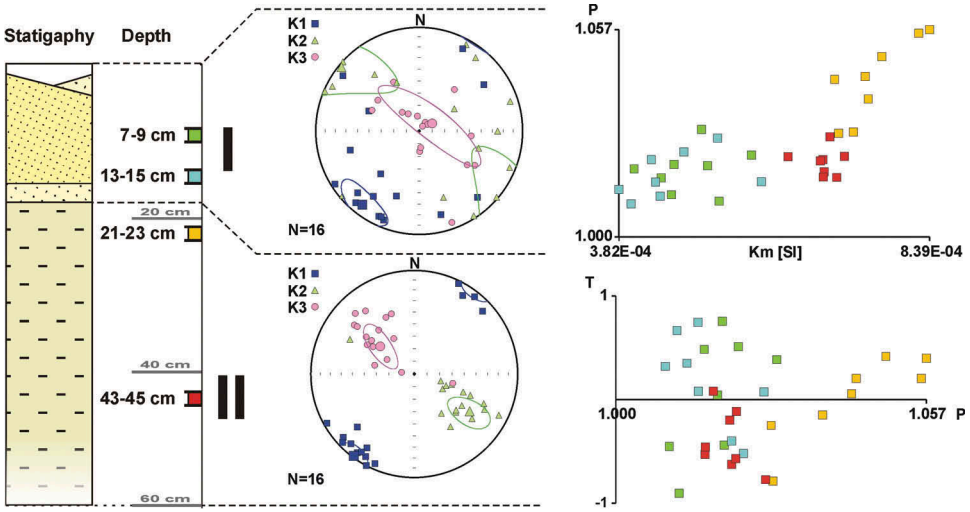

Figure 4. AMS results in relation to stratigraphy: I – upper horizon; II – lower horizon. Principal susceptibility directions (K_1, K_2, K_3) in geographic coordinate system are plotted to equal area projection on the lower hemisphere. Green, blue, yellow, and red squares in Jelinek plots represent results of samples from depths 7–9, 13–15, 21–23, and 43–45 cm. For stratigraphy explanation, see Figure 2.

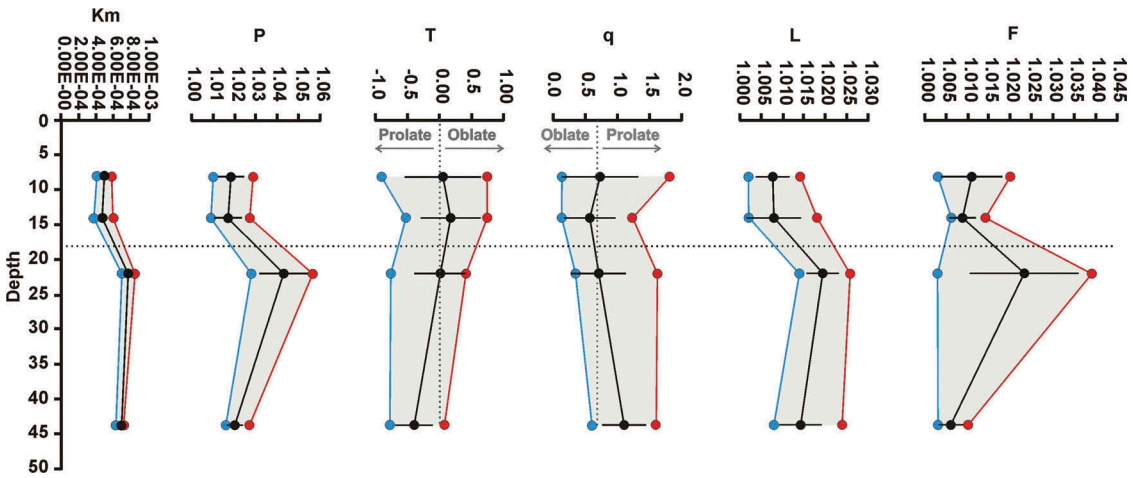

Figure 5. Horizontal variability of parameters based on eight samples for each sampled depth-interval vs. profile-depth at Las Salinas 004 site. Maximal (red), minimal (blue), and mean (black) values of individual parameters as well as standard deviation (horizontal black lines) are shown. K_m – mean bulk magnetic susceptibility in SI units; P – degree of anisotropy; T – shape parameter; q – shape factor; L – magnetic lineation; F – magnetic foliation.

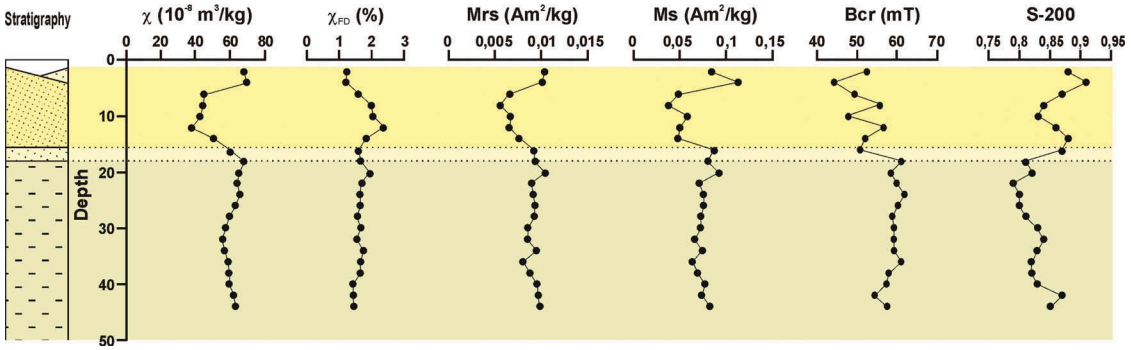

Figure 6. Rock magnetic parameters vs. depth. Key: mass specific magnetic susceptibility (x), frequency-dependent susceptibility (x_{fd}), and other hysteresis parameters (M_{rs}, M_s, B_{cr}, and S_{-200}).

the top of the upper unit, the values reach their maximum followed by a relatively rapid decrease yielding the minimum number of parameters in the middle part of this layer. Approaching the bottom of this unit, the values increase again. This behaviour differs from that observed in the lower unit. In this part of the profile, the values of χ, M_{rs}, and M_s are more homogeneous with almost no variations, although a minimum at 32 cm may be observed mainly in the susceptibility profile. Therefore, the observed variations in magnetic properties are roughly controlled by the lithology, being the concentration of ferromagnetic minerals lower in the upper sand units than in the deeper clay units.

Although frequency-dependent susceptibility values are very low (Figure 6), less than 3% in the whole profile, the most important variations can be observed in the upper unit. These values indicate that the contribution of superparamagnetic (SP) ferrimagnetic minerals is minor along the entire profile and mainly in the upper part.

A well-marked difference in remanent coercivity values (B_{cr}) can be distinguished between the upper and lower units (Figure 6). The values in the upper unit are somewhat lower and exhibit greater variation than those in the lower unit. Whereas the mean coercivity value in the upper unit is 51.1 mT, the lower unit shows a mean of 59.1 mT. The specific parameter, S_{-200} was calculated on the basis of the equation $S_{-200} = ((-IRM_{-0.2\ T}/SIRM) + 1)/2$ following Bloemendal *et al*. (1992), and computed using RockMagAnalyzer 1.0 software (Leonhardt 2006). $IRM_{-0.2\ T}$ and SIRM denote the isothermal remanent magnetization at a reversed field of 0.2 and 1 T, respectively. This parameter roughly yields the relative contribution of high-coercivity minerals in a mixture with ferrimagnetic minerals. Because high-coercivity minerals do not fully saturate at the maximum applied field of 1 T, it is quite possible that the value is biased due to the proportion of these high-coercivity minerals. The values of S_{-200} in the upper unit vary between 0.89 and 0.82, and in the lower unit between 0.84 and 0.79 (except at depth 42 cm). This difference in coercivity can also be observed from Figure 7, suggesting a higher contribution of a hard magnetic phase in the lower unit. Samples 004–4 (7–9 cm) and 004–6 (11–13 cm), from the upper unit, with highest B_{cr} values and extreme values of M_{rs}/χ, are seen in Figure 7.

The magnetization and coercivity ratios (M_{rs}/M_s and B_{cr}/B_c, respectively) were plotted on Day plots (Figure 8 (a) and (b); Day *et al*. 1977). The values of the hysteresis ratio for two representative samples of layers 004–04 (7–9 cm) and 004–19 (37–39 cm) are indicated in the Day plots. Two different trends corresponding to each

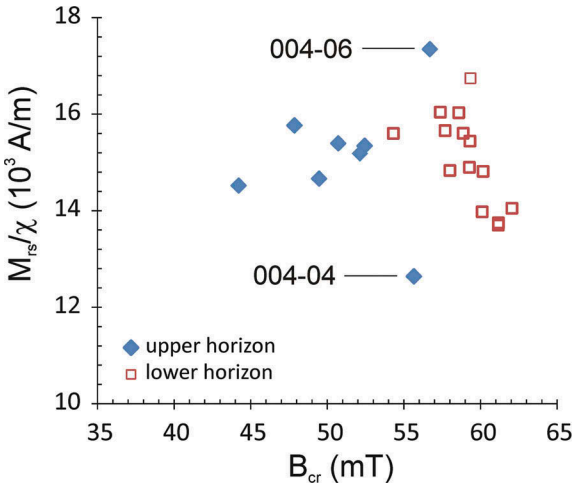

Figure 7. Bi-plot of saturation remanent magnetization/susceptibility (M_{rs}/χ) vs. the coercivity of remanence (B_{cr}). Two exceptional samples for the upper unit are indicated.

unit can be distinguished, both in the magnetite pseudo-single-domain (PSD) area. Samples from the upper unit follow the theoretical hysteresis trend for the SD+MD (multi-domain) mixing model curve, but plotted parallel and above it (Figure 8(b)). However, samples from the lower unit mainly exhibit variations in the B_{cr}/B_c ratio. Although in terms of B_{cr}/B_c there is an overlap, most samples from the lower unit show higher coercivity ratios than the upper one. The observed behaviour can be explained as a mixture of SD and multi-domain (MD) magnetite and/or titanomagnetite particles, since the values are closer to the SD+MD trend (Dunlop 2002). The displacement from the theoretical trend probably cannot be explained by a contribution of SP magnetite and/or titanomagnetite grains, since the obtained values of frequency dependence susceptibility (χ_{fd}) indicate that the presence of these grains is not significant. Saturation remanence/saturation magnetization ratios M_{rs}/M_s and coercivity ratios B_{cr}/B_c are M_{rs}/M_s = 0.5–0.9, B_{cr}/B_c = 1.02–1.17 for MD haematites (Fe_2O_3) and M_{rs}/M_s = 0.5–0.7, B_{cr}/B_c = 1.45–1.62 for SD Fe_2O_3 (Özdemir and Dunlop 2014). Therefore, if samples also include Fe_2O_3 grains, and depending on their relative concentration, the shape of the distribution of the hysteresis parameter ratios on the Day plot would be affected.

The hysteresis loops and isothermal remanent acquisition curves (M_r or *IRM*) for two representative samples from both upper and lower units are plotted in Figure 8 (c) and (d). The hysteresis loops are plotted before and after correction for paramagnetic contribution. Despite the presence of high-coercivity minerals, from visual assessment the corrected hysteresis loops show no evidence of a mixture of minerals of varying coercivity.

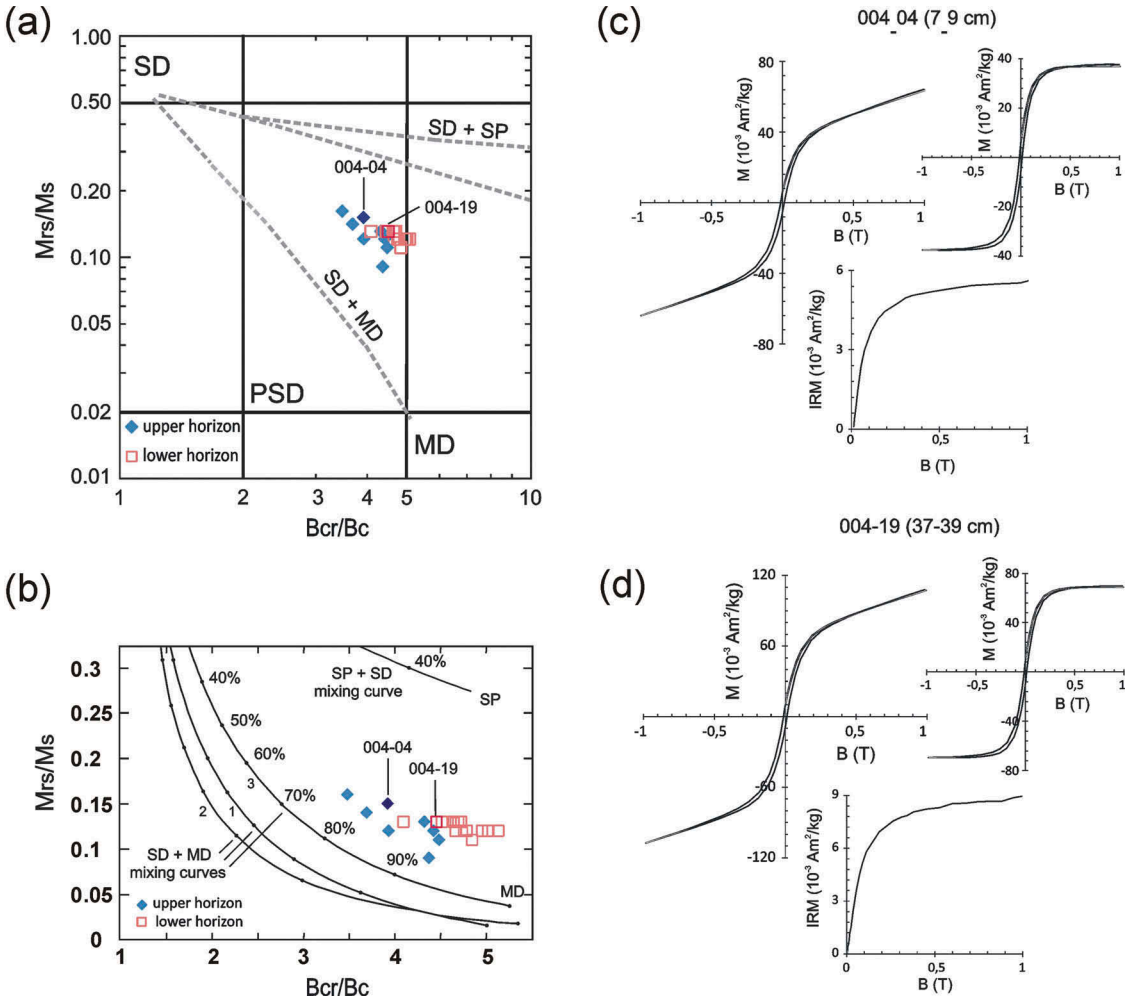

Figure 8. Results of hysteresis studies: (a) hysteresis parameters M_r/M_s and B_{cr}/B_c plotted on a Day plot in logarithmic scale (Day *et al*. 1977) for samples from upper (solid diamonds) and lower units (open squares), modified from Dunlop (2002). Dashed lines represent mixing curves for mixtures of single-domain (SD) with superparamagnetic domain (SP) or multi-domain (MD); (b) detailed Day plot in lineal scale with the theoretical mixing curves for SD+MD and SD+SP. The results of two representative samples are indicated in the plot; (c) hysteresis loops for upper unit sample; and (d) lower unit sample with insets of loops corrected for paramagnetic contributions and isothermal remanent magnetization curves.

However, the obtained values of B_c may have been affected by bias. Isothermal remanent acquisition curves (M_r) do not saturate at the maximum applied field of 1 T in the whole profile, since the high-field slope is steeper for samples from the lower layer. In order to improve the determination of the magnetic carries, additional IRM acquisition curves up to 2 T by conducting pulse magnetometry on the field were performed. In this case, we show the IRM acquisition plots and gradient curves for three examples corresponding to the upper layer (7–9 cm), lower layer (37–39 cm), and the contact between them (17–19 cm) (Figure 9). Since this experiment was carried out on the twin samples shown in Figure 8, small differences can be observed in IRM values. Modelling of IRM acquisition data clearly discriminates two magnetic phases in all samples. The main magnetic carrier is a low-coercivity phase (component 1) with mean coercivity ($B_{1/2}$) values between 53.2 and 58.9 mT, probably corresponding to (titano)magnetite/(titano)maghaemite. The high-coercivity phase (component 2) with $B_{1/2}$ values between 273.5 and 335 mT may be attributed to Fe_2O_3, since this phase is also identified in the thermomagnetic experiments. Comparing the curves, certain differences can be observed. First, although the SIRM values (total concentration of ferromagnetic minerals) are higher in the lower unit than in the upper, the relative contribution to each sample of the low-coercivity phase is higher in samples from the upper layer (sand units). Second, the contribution of the high-coercivity phase is greater and slightly harder (magnetically) in the lower layer (clay units) than the upper. On the other hand, the wide shape of these two peaks indicates major variations in grain size and/or composition of the iron oxide crystals, suggesting detrital components.

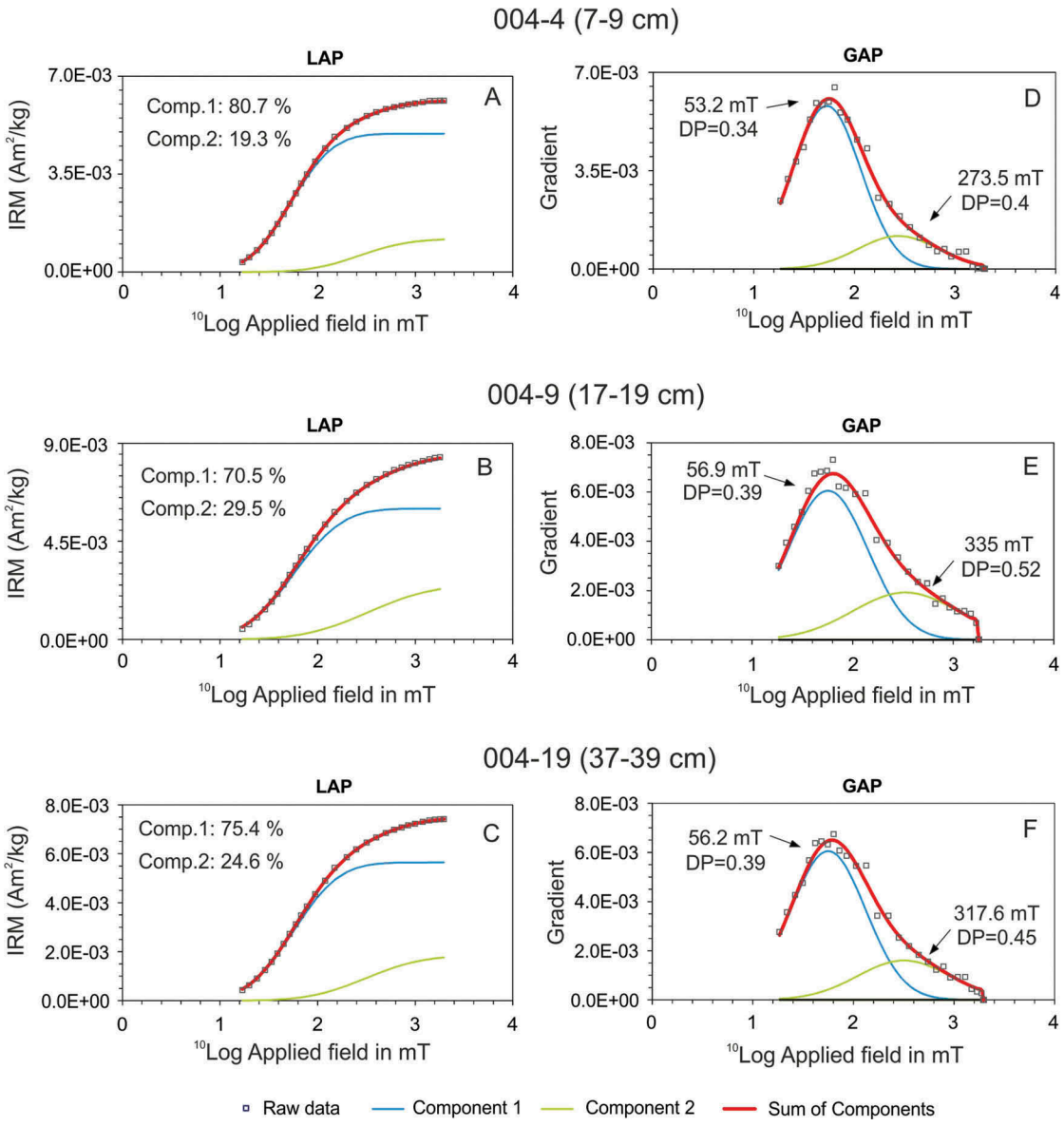

Figure 9. IRM component analysis was carried out following Kruiver *et al*. (2001) and Heslop *et al*. (2002) for three representative examples of the upper unit (004–4), the contact layer between the upper and lower units (004–9), and the lower unit (004–19). Plots A–C and D–F correspond to the linear acquisition plots (LAP) and the gradient acquisition plots (GAP), respectively.

3.4. ^{210}Pb and ^{137}Cs chronologies

^{210}Pb ($^{210}Pb_{total}$, $^{210}Pb_{sup}$, and $^{210}Pb_{xs}$) and ^{137}Cs activities are shown in Figure 10. $^{210}Pb_{xs}$ and ^{137}Cs activity in Sal-005 showed atypical profiles, which precludes the use of these data to obtain geochronology. However, two relevant observations can be drawn: (1) $^{210}Pb_{xs}$ activity is detectable in sediments up to 15 cm depth, which implies that these sediments are younger than 110 years (equivalent to five times the half-life of ^{210}Pb); (2) there is also detectable activity in ^{137}Cs in several sections of the core (higher than the minimal detectable activity of 2 Bq kg^{-1}) above 6 cm depth, which implies that these sediments were deposited since the 1950s (when atmospheric nuclear testing began and the artificial radionuclide ^{137}Cs became detectable globally).

4. Discussion

Recently published papers, and not only those focused on the study of marine inundation deposits, generally use AMS parameters with no statistical evaluation of lateral variability (or dispersivity) in the properties of sedimentary layers (e.g. Wassmer *et al*. 2010; Goguitchaichvili *et al*. 2013; Schneider *et al*. 2014; Zeeden *et al*. 2015). AMS parameters are always calculated from values of principal susceptibilities (K_1, K_2, and

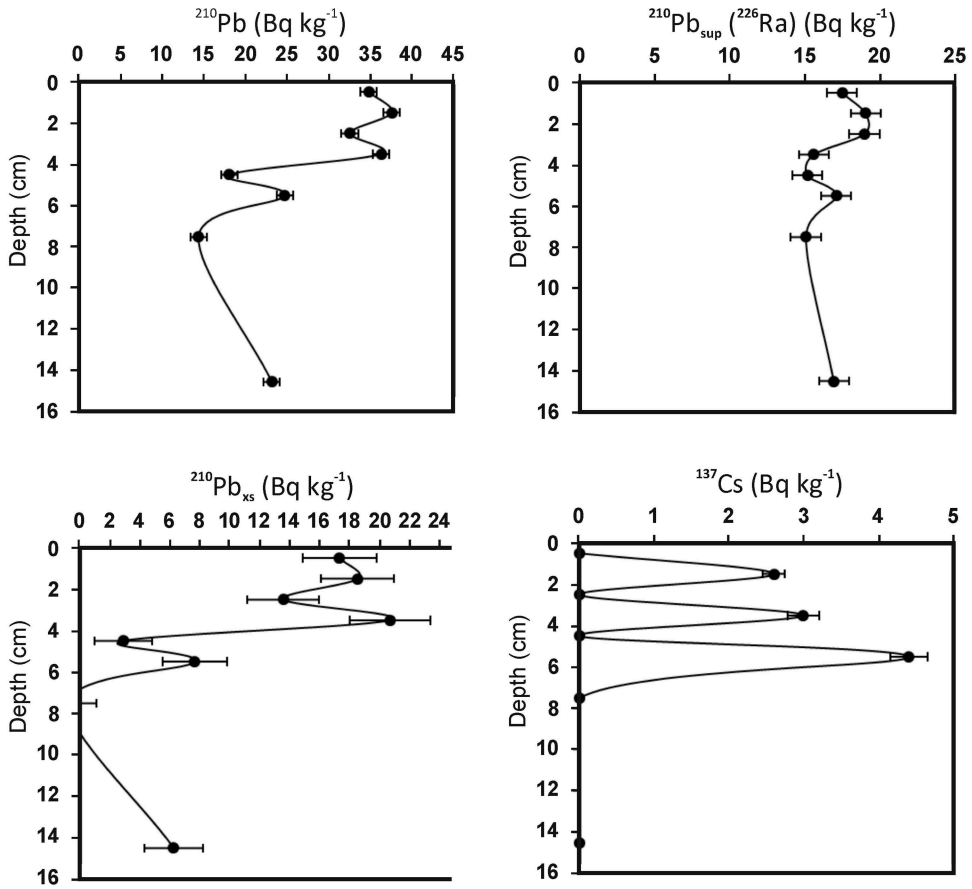

Figure 10. ^{210}Pb (^{210}Pb$_{total}$, ^{210}Pb$_{sup}$, and ^{210}Pb$_{xs}$) and ^{137}Cs activity depth distribution profiles from Sal005. ^{210}Pb$_{sup}$ was determined as ^{226}Ra (assuming secular equilibrium between the two radionuclides), and ^{210}Pb$_{xs}$ was obtained from the difference between ^{210}Pb$_{total}$ and ^{210}Pb$_{sup}$.

K_3). However, differences between maximal and minimal values are very small and it should be taken into account that any minor change can strongly affect AMS properties, at least in the case of sedimentary layers deposited by high-velocity currents where significant horizontal variations are expected (reorientation of non-spherical grains due to turbulent flow, grain size variations, presence of rip-up clasts, etc.).

Two different ways of sampling were used for this purpose. The standard method of sampling along a vertical profile was used for determination of the main carriers of MS (thermomagnetic curves) and the observation of variations with depth in MS, frequency-dependent susceptibility, and hysteresis parameters. The second method of sampling in the horizontal direction was used for a pilot study of horizontal variability of AMS parameters.

4.1. Magnetic minerals and their source

Thermomagnetic curves (x–*T*) showed differences between two units, and these helped to determine the two main carriers of MS. Temperatures between 575 and 585°C correspond to the Curie point of magnetite, but lower Curie temperatures may correspond to several minerals with variable Ti content, such as titanomagnetite, titanomaghaemite, or titanohaematite. We assume that the source of minerals with a variable content of Ti was probably volcanic material produced by volcanoes related to the Mexican active margin. This idea is strongly supported by comparison of our results to previous thermomagnetic studies on tephra samples (Figure 11). Tephras were analysed in the neighbouring Michoacán area, where titanomagnetite was identified (Ortega *et al.* 2002).

Titanomagnetite represents a complete solid solution between two marginal members – magnetite (Fe_3O_4) and ulvöspinel (Fe_2TiO_4). The Curie temperature of titanomagnetite depends on the proportions of Ti and Fe, and may vary between −150 and 580°C (Akimoto *et al.* 1957; Nagata 1961). The wide range of Curie temperatures between 350 and 585°C in the lower unit most probably reflects sediment containing both magnetite and titanomagnetite with a variable range of Ti from 0 to 30% of the component. Such curve characteristics, as in tephras, where a gradual drop can be observed,

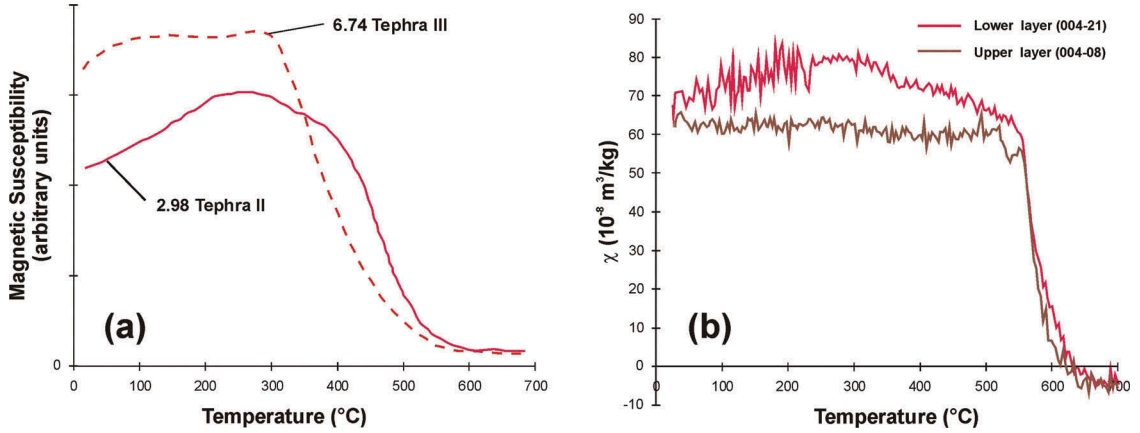

Figure 11. Heating curves of magnetic susceptibility vs. temperature for: (a) tephra samples from Michoacán (after Ortega *et al.* 2002, modified); (b) sediment samples from the upper and lower layers. The thermomagnetic curves from both tephra and sediment samples have a very similar character, especially samples tephra-II and 004–21 from the lower unit (measured under argon atmospheric conditions).

possibly followed by a sharp decrease, is typical for volcanic material with finer grains of titanomagnetite and is a result of diffusive fractionation (Zhou *et al.* 2000). Therefore, the final proportions of Ti and Fe in titanomagnetite most probably depend on the initial content of Ti and Fe in the melt as well as the rate of cooling. For this reason, the character of the curve should be considered rather than the exact Curie temperatures. Nevertheless, it is not possible to exclude participation of other sources for pure magnetite.

Similar characteristics of the heating curves of the tephra-II sample (Figure 11(a)) and lower unit (represented by sample 004–21; Figure 11(b)) are evident. Titanomagnetite with a variable Ti content was demonstrated in a tephra-II sample (Ortega *et al.* 2002), and we assume that this is also responsible for the variable range of Curie temperature in sample 004–21. However, titanomagnetite is not the only potential mineral which might be considered as the main carrier of MS in this case. Titanohaematite also represents a complete solid solution between Fe_2O_3 and ilmenite ($FeTiO_3$), where Néel temperatures may also vary over a wide range between −220 and 675°C depending on Ti content (Nagata 1961; Stacey and Banerjee 1974). However, the gradual, uninterrupted drop of the curve related to sample 004–21, followed by a sharp decrease due to the Curie temperature of magnetite, suggest that: (1) the mineral with a variable Ti content is part of a magnetite–ulvöspinel complete solid solution (i.e. titanomagnetite); and (2) the major proportion of magnetite grains might be of the same origin as titanomagnetites, and we consider this as possible evidence that material of volcanic origin significantly contributed to the main carriers of MS in the studied sediments at Las Salinas site. In addition, in a few samples mainly from the lower unit, it is possible to identify a phase with Curie/Néel temperature above 650°C, probably Fe_2O_3.

The magnetic parameters show variation in behaviour between the upper and lower layers. The rough correlation among χ, M_{rs}, and M_s (Figure 6) indicates that the concentration of ferrimagnetic minerals (magnetite and/or titanomagnetite) dominates such variation in this profile. Differences among these three parameters, mainly in the upper unit, could be due to the contribution of high-coercivity minerals and/or to variation in grain size distribution. Indeed, higher discrepancies between χ and M_s can be observed in the upper unit between 8 and 12 cm, precisely where the contribution of ferrimagnetic minerals is minimal and the relative contribution of high-coercivity minerals (Fe_2O_3 and/or titanohaematite) has a well-defined maximum, as indicated by the S_{-200} ratio (Figure 6). For example, sample 004–06 (11–13 cm) shows the highest value of SIRM/χ and higher coercivity compared with other samples from the upper unit (Figure 7), probably indicating a major contribution of Fe_2O_3 (Thompson and Oldfied 1986). On the other hand, sample 004–04 (7–9 cm) exhibits the lowest value of SIRM/χ, possibly related to an increase in the relative contribution of MD magnetite and/or titanomagnetite. Therefore, variable fractions of high-coercivity minerals (probably Fe_2O_3 and/or titanohaematite) and (titano)magnetite grain size distribution are detectable along the upper unit, as also observed in Day plots (Figure 8).

In the lower unit, the absolute concentration of soft magnetic minerals is higher than in the upper (Figure 6). Increase in the ratio S_{-200} with depth indicates that the relative concentration of Fe_2O_3 (and/or titanohaematite) decreases correspondingly. In addition the parameter B_{cr} is quite uniform, showing a slight decrease with

depth. The major concentration of high-coercivity minerals is found in the lower unit, since the values of S_{-200} in this unit are lower than in the upper (the only exception being the bottom of the profile). This behaviour was also observed from statistical analysis of the IRM (Figure 9), since the percentage of the high-coercivity component is higher in the lower than in the upper unit and decreases with depth.

4.2. Variability of AMS parameters and mean susceptibility

The horizontal variability of AMS parameters in sedimentary layers is usually underestimated; indeed, it can be very low in some sediments. However, without testing of individual beds/horizons it cannot be determined whether it significantly affects the results or not. The only way to be certain is to test by collecting several samples in the same horizon. This test is even more suitable when a high lateral variability is expected, as in the case of marine inundation deposits. To understand the problem of lateral variability of AMS parameters, it must be understood that (1) the AMS ellipsoid of sediments has almost a spherical geometry and (2) AMS parameters are always enumerated from the length (K_1, K_2, and K_3) of vectors $\mathbf{K_1}$, $\mathbf{K_2}$, and $\mathbf{K_3}$ representing principal susceptibility directions (semi-axes of the AMS ellipsoid). In general, the degree of anisotropy ($P = K_1/K_3$) of depositional sedimentary fabrics usually has values less than 1.05 (i.e. anisotropy <5%; Weiler 2007). This means that the difference between the maximal susceptibility K_1 and K_3 is usually less than 5%, and the ellipsoid is almost represented by a spherical geometry. Therefore, the lateral variability of AMS parameters in sedimentary layers can be significant as in the case of Las Salinas site.

Two almost equivalent parameters, T and q, are generally used in recently published papers. These parameters describe the geometry of the AMS ellipsoid ($-1 \leq T < 0$ – prolate; $0 < T \leq 1$ – oblate; $q > 0.63$ – prolate; $q < 0.63$ – oblate). Results from Las Salinas locality show an extreme range of T and q parameter values representing both oblate and prolate shapes (Figure 5). This implies that we can randomly obtain parameter values representing an oblate or prolate shape of the AMS ellipsoid without statistical evaluation of the shape in each horizon. As our results suggest, testing of horizontal variability in sedimentary layers should be performed before final interpretations.

Only the K_m value provides reliable results without wider statistical horizontal analysis in this case, but from the geological point of view, if we plot K_m value against depth, it gives us almost the same information as the other measurements of total MS. Maximal horizontal variability of the other parameters in relation to depth is obvious from the results. The range is given by the generally overlooked lateral variability of sediments.

4.3. AMS fabrics

Even though samples were taken from four individual horizons, only two magnetic fabrics were distinguished. The data from the two uppermost horizons related to depths of 7–9 and 13–15 cm show overlapping of $\mathbf{K_1}$, $\mathbf{K_2}$, and $\mathbf{K_3}$, directions as well as data in both Jelinek diagrams (blue and green squares, Figure 4). The similar patterns of AMS and lithology are reasons why it was possible to unify these as fabric type I. The second magnetic fabric type shows even better overlapping of $\mathbf{K_1}$, $\mathbf{K_2}$, and $\mathbf{K_3}$ directions in the equal area projection. On the other hand the data in the Jelinek diagrams related to depths 21–23 and 43–45 cm show two individual clusters (yellow and red squares, Figure 4). However, a slight upwards increase in K_m values suggests possible vertical changes in incoming clay-sized particles rather than dynamical changes in flow parameters. These changes are subtle and are not observable in sedimentary records. Moreover, magnetic fabric I shows a much higher dispersal of the shape parameter T and a relatively lower degree of anisotropy P in comparison with magnetic fabric II (Jelinek P–T diagram, Figure 4). Such differences are related to lithology (sand – higher dispersal of T and lower P values; clay – lower dispersal of T and higher P values).

Previous studies of magnetic fabrics in relation to depositional processes have shown that the clustering of $\mathbf{K_1}$ directions is related to the flow direction or inclination of the slope during deposition, and the orientation of mean $\mathbf{K_3}$ direction is usually perpendicular to the bedding, tilted in the direction of the flow or scattered in the case of primary sedimentary fabrics (e.g. Rees and Woodall 1975; Ellwood and Ledbetter 1977; Taira and Scholle 1979; Taira 1989; Tarling and Hrouda 1993). Therefore, we consider the mean $\mathbf{K_1}$ direction as a representative direction of flow for fabrics I and II. However, both horizons related to fabric II show a significant inclination of the $\mathbf{K_3}$ direction of about 35° from vertical in a direction perpendicular to the flow direction (represented by $\mathbf{K_1}$; Figure 4). Assuming that the bottom clay unit was not affected by any post-depositional deformation, we have to consider that the magnetic fabric resulted solely from sedimentary processes.

Sedimentary processes potentially leading to origination of the fabric with lateral imbrication have been described in coarse-grained sediments, such as gravel or sand in braided rivers, where traction played a

significant role (e.g. Williams and Rust 1969; Teisseyre 1975; Allen 1983; Yagishita 1997). However, we cannot use such an explanation for clay sediments as long as they are deposited in a horizontal plane. Assuming that the lagoon was supplied with freshwater streams from inland, then the water must have been drained towards the sea and water channels could have been developed. In recent analogues, such channels can have steep rims and they can provide ideal conditions for the origin of laterally imbricated fabric in clays. Rills with high-sinuosity configuration can be developed also in flat tidal areas composed of silt and clay. In such an environment, the rills can migrate laterally and form point bars with accretionary surfaces dipping at angles of over 20° (Vilas *et al*. 1999). Considering the position of the lagoon and sampling site Las Salinas 004 (Figure 1), we may also speculate about the described tidal area scenario. Visualization of magnetic fabric II in a block diagram shows prolongation of magnetic carriers parallel to magnetic lineation (indicating flow direction) and lateral imbrication indicated by inclination of magnetic foliation (Figure 12).

Magnetic fabric I has almost the same orientation of mean $\mathbf{K_1}$ direction (Figure 4) but a significant reorientation tendency to perpendicular position, and a higher degree of scattering of $\mathbf{K_2}$ and $\mathbf{K_3}$ suggests that this unit was deposited in a higher-energy environment than the lower one (e.g. Ellwood and Ledbetter 1977; Taira and Scholle 1979; Tarling and Hrouda 1993). Such relation between flow direction and direction $\mathbf{K_1}$ was also reported in recent studies of tsunami deposits (e.g. Wassmer *et al*. 2010; Cuven *et al*. 2013; Schneider *et al*. 2014). The slightly lower MS of the fabric cannot justify greater scatter in the orientations of the principal susceptibility directions in this case. The MS is still sufficiently high and cannot be considered as the reason for measurement error.

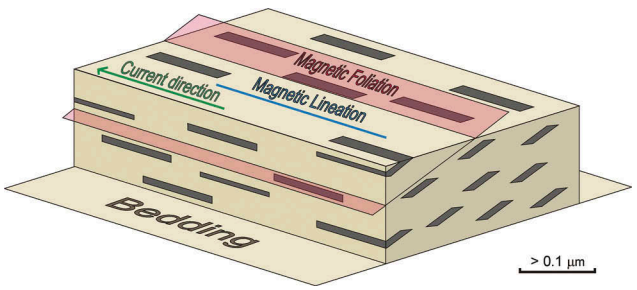

Figure 12. Schematic visualization of magnetic fabric II recognized in the lower unit. The magnetic fabric suggests that lateral imbrication of magnetic particles was developed in the sediment.

4.4. Age of the deposits

The upper sand unit (1–18 cm) was dated by ^{210}Pb and ^{137}Cs radionuclide chronology. Although these techniques did not provide specific dates, the presence of ^{210}Pb in excess activities in the upper 15 cm of the core indicated that the sediments are younger than 110 years, and thus the upper section could be the result of either tsunami (1932 or 1995) that affected this area, or even of one of the several storms that have also hit this section of the coast during the last 110 years. However, the 1995 event produced by an earthquake measured as Mw 8.0 and a tsunami with a maximum run-up of 5.1 m was relatively small, and it is unlikely that it could have produced a 17 cm sand layer 900 m from the coast. The 1932 event (Ms = 8.2) was a larger tsunami that flooded several locations on the Jalisco and Colima coast, including the study site. Therefore, this is perhaps the most likely candidate for the deposition of the upper sand layer. We cannot exclude the possibility of storm deposits; however, based on the distance of the deposit from the shore (almost 1 km), it is very unlikely that this deposit was laid down by a storm.

5. Conclusions

Even though magnetic studies alone cannot help solve the question of whether a marine inundation deposit was laid down by a tsunami or a storm event, these can significantly help to answer other important questions. The results from Las Salinas showed that magnetic studies may help us understand the following. (1) Material of volcanic provenance was a significant source of magnetic minerals in the lower clay layer. (2) Magnetic fabric related to the lower unit suggests that the unit developed lateral imbrication. Although such structures have been poorly studied, sedimentology indicates that the unit was deposited in a low-energy environment not related to a tsunami event. (3) Statistical evaluation of principal susceptibility directions suggests that the upper unit was deposited in a higher-energy environment than the lower unit. (4) As indicated by the results from Las Salinas, the lateral variability of AMS parameters at an outcrop scale may be very wide. The usage of only a single value of certain AMS parameter without statistical evaluation cannot be considered representative for a certain depth and may give random and false results. This implies that the variability can sometimes be very significant, and testing of horizontal variability in sedimentary layers should be performed before final interpretations. (5) Despite the

uncertainties in data, we believe that the origin of the upper unit at the study site is most probably related to the tsunami event of 3 June 1932.

Acknowledgement

The authors acknowledge the technical assistance of L.H. Perez Bernal in gamma spectrometry measurements.

Disclosure statement

No potential conflict of interest was reported by the authors.

Funding

J. Černý acknowledges financial support by the Mexico Government student exchange programme Secretaria de Relaciones Exteriores de México and the institutional support assigned as RVO:67985831. M.T. Ramírez-Herrera acknowledges financial support by SEP-CONACYT research grant 129456. M.F. Bógalo acknowledges financial support by the projects CGL2012-38481 and CGL2012-32149 of the Dirección General de Investigación Científica y Técnica, Ministerio de Economía y Competitividad of the Spanish government and European Regional Development Fund. A. Goguitchaichvili acknowledges the financial support of UNAM PAPIIT IN105214. R. Castillo-Aja acknowledges PhD scholarship by CONACYT.

References

Akimoto, S., Katsura, T., and Yoshida, M., 1957, Magnetic properties of the Fe_2TiO_4–Fe_3O_4 system and their change with oxidation: Journal of Geomagnetism and Geoelectricity, v. 9, p. 165–178. doi:10.5636/jgg.9.165

Allen, J.R.L., 1983, Studies in fluviatile sedimentation: Bars, bar-complexes and sandstone sheets (low-sinuosity braided streams) in the Brownstones (L. Devonian), Welsh Borders: Sedimentary Geology, v. 33, p. 237–293. doi:10.1016/0037-0738(83)90076-3

Appleby, P.G., 1998, Dating recent sediments by 210Pb: Problems and solutions, *in* Proceedings, dating of sediments and determination of sedimentation rate, Helsinki, 2–3 April 1997: Helsinki, Finnish Centre for Radiation and Nuclear Safety, STUK-A145, p. 7–24.

Bloemendal, J., King, J.W., Hall, F.R., and Doh, S.J., 1992, Rock magnetism of Late Neogene and Pleistocene deep-sea sediments: Relationship to sediment source: Diagenetic processes and sediment lithology: Journal of Geophysical Research, v. 97, no. B4, p. 4361–4375.

Borerro, J., Ortiz, M., Titov, V., and Synolakis, C., 1997, Field survey of Mexican tsunami produces new data, unusual photos: EOS transactions: American Geophysical Union, v. 78, no. 8, p. 85–88. doi:10.1029/97EO00054

Chagué-Goff, C., Goff, J., Nichol, S.L., Dudley, W., Zawadzki, A., Bennett, J.W., Mooney, S.D., Fierro, D., Heijnis, H., Dominey-Howes, D., and Courtney, C., 2012, Multi-proxy evidence for trans-Pacific tsunamis in the Hawai'ian Islands: Marine Geology, v. 299–302, p. 77–89. doi:10.1016/j.margeo.2011.12.010

Chagué-Goff, C., Schneider, J.-L., Goff, J.R., Dominey-Howes, D., and Strotz, L., 2011, Expanding the proxy toolkit to help identify past events—Lessons from the 2004 Indian Ocean Tsunami and the 2009 South Pacific Tsunami: Earth-Science Reviews, v. 107, p. 107–122. doi:10.1016/j.earscirev.2011.03.007

Corona, N., and Ramírez-Herrera, M.T., 2012a, Mapping and historical reconstruction of the great Mexican 22 June 1932 tsunami: Natural Hazards and Earth System Sciences, v. 12, no. 5, p. 1337–1352. doi:10.5194/nhess-12-1337-2012

Corona, N., and Ramírez-Herrera, M.T., 2012b, Técnicas histórico-etnográficas en la reconstrucción y caracterización de tsunamis: El ejemplo del gran tsunami del 22 de junio de 1932, en las costas del Pacífico Mexicano: Revista de Geografía Norte Grande, v. 53, p. 107–122. doi:10.4067/S0718-34022012000300007

Cuven, S., Paris, R., Falvard, S., Miot-Noirault, E., Benbakkar, M., Schneider, J.-L., and Billy, I., 2013, High-resolution analysis of a tsunami deposit: Case-study from the 1755 Lisbon tsunami in southwestern Spain: Marine Geology, v. 337, p. 98–111. doi:10.1016/j.margeo.2013.02.002

Day, R., Fuller, M., and Schmidt, V.A., 1977, Hysteresis properties of titanomagnetites: Grain-size and compositional dependence: Physics of the Earth and Planetary Interiors, v. 13, p. 260–267. doi:10.1016/0031-9201(77)90108-X

Dearing, J.A., Dann, R.J.L., Hay, K., Lees, J.A., Loveland, P.J., Maher, B.A., and O'Grady, K., 1996, Frequency-dependent susceptibility measurements of environmental materials: Geophysical Journal International, v. 124, p. 228–240. doi:10.1111/gji.1996.124.issue-1

DeLaune, R.D., Patrick, W.H., and Buresh, R.J., 1978, Sedimentation rates determined by ^{137}Cs dating in a rapidly accreting salt marsh: Nature, v. 275, p. 532–533. doi:10.1038/275532a0

Dunlop, D.J., 2002, Theory and application of the Day plot (M_{rs}/M_s versus H_{cr}/H_c), 1. Theoretical curves and tests using titanomagnetite data: Journal of Geophysical Research, v. 107, no. B3, p. EPM 4 1–22. doi:10.1029/2001JB000486.

Ellwood, B.B., and Ledbetter, M.T., 1977, Antarctic bottom water fluctuations in the vema channel: Effects of velocity changes on particle alignment and size: Earth and Planetary Science Letters, v. 35, p. 189–198. doi:10.1016/0012-821X(77)90121-2

Ferrari, L., Orozco-Esquivel, T., Manea, V.C., and Manea, M., 2012, The dynamic history of the Trans-Mexican Volcanic Belt and the Mexico subduction zone: Tectonophysics, v. 522–523, p. 122–149. doi:10.1016/j.tecto.2011.09.018

Font, E., Nascimento, C., Omira, R., Baptista, M.A., and Silva, P. F., 2010, Identification of tsunami-induced deposits using numerical modeling and rock magnetism techniques: A study case of the 1755 Lisbon tsunami in Algarve, Portugal: Physics of the Earth and Planetary Interiors, v. 182, p. 187–198. doi:10.1016/j.pepi.2010.08.007

Font, E., Veiga-Pires, C., Pozo, M., Nave, S., Costas, S., Ruiz Muñoz, F., Abad, M., Simões, N., Duarte, S., and Rodríguez-Vidal, J., 2013, Benchmarks and sediment source(s) of the 1755 Lisbon tsunami deposit at Boca do Rio Estuary: Marine Geology, v. 343, p. 1–14. doi:10.1016/j.margeo.2013.06.008

Goguitchaichvili, A., Ramírez-Herrera, M.T., Calvo-Rathert, M., Aguilar Reyes, B., Carrancho, Á., Caballero, C., Bautista, F., and Morales Contreras, J., 2013, Magnetic fingerprint of

tsunami-induced deposits in the Ixtapa–Zihuatanejo Area, Western Mexico: International Geology Review, v. 55, p. 1462–1470. doi:10.1080/00206814.2013.779781

Granar, L., 1958, Magnetic measurements on Swedish varved sediments: Arkiv För Geofysik, v. 3, p. 1–40.

Grommé, C.S., Wright, T.L., and Peck, D.L., 1969, Magnetic properties and oxidation of iron-titanium oxide minerals in Alae and Makaopuhi Lava Lakes, Hawaii: Journal of Geophysical Research, v. 74, p. 5277–5293. doi:10.1029/JB074i022p05277

Heslop, D., Dekkers, M.J., Kruiver, P.P., and Van Oorschot, I.H. M., 2002, Analysis of isothermal remanent magnetization acquisition curves using the expectation-maximization algorithm: Geophysical Journal International, v. 148, p. 58–64. doi:10.1046/j.0956-540x.2001.01558.x

Jankaew, K., Atwater, B.F., Sawai, Y., Choowong, M., Charoentitirat, T., Martin, M.E., and Prendergast, A., 2008, Medieval forewarning of the 2004 Indian Ocean tsunami in Thailand: Nature, v. 455, p. 1228–1231. doi:10.1038/nature07373

Jelinek, V., 1981, Characterization of the magnetic fabric of rocks: Tectonophysics, v. 79, p. T63–T67. doi:10.1016/0040-1951(81)90110-4

Kamatani, A., 1982, Dissolution rates of silica from diatoms decomposing at various temperatures: Marine Biology, v. 68, p. 91–96. doi:10.1007/BF00393146

Kench, P.S., McLean, R.F., Brander, R.W., Nichol, S.L., Smithers, S.G., Ford, M.R., Parnell, K.E., and Aslam, M., 2006, Geological effects of tsunami on mid-ocean atoll islands: The Maldives before and after the Sumatran tsunami: Geology, v. 34, p. 177–180. doi:10.1130/G21907.1

Kench, P.S., Nichol, S.L., Smithers, S.G., McLean, R.F., and Brander, R.W., 2008, Tsunami as agents of geomorphic change in mid-ocean reef islands: Geomorphology, v. 95, p. 361–383. doi:10.1016/j.geomorph.2007.06.012

Khan, M.A., 1962, The anisotropy of magnetic susceptibility of some igneous and metamorphic rocks: Journal of Geophysical Research, v. 67, p. 2873–2885. doi:10.1029/JZ067i007p02873

Kortekaas, S., and Dawson, A.G., 2007, Distinguishing tsunami and storm deposits: An example from Martinhal, SW Portugal: Sedimentary Geology, v. 200, p. 208–221. doi:10.1016/j.sedgeo.2007.01.004

Krishnaswamy, S., Lal, D., Martin, J., and Meybeck, M., 1971, Geochronology of lake sediments: Earth and Planetary Science Letters, v. 11, p. 407–414. doi:10.1016/0012-821X(71)90202-0

Kruiver, P.P., Dekkers, M.J., and Heslop, D., 2001, Quantification of magnetic coercivity components by the analysis of acquisition curves of isothermal remanent magnetisation: Earth and Planetary Science Letters, v. 189, p. 269–276. doi:10.1016/S0012-821X(01)00367-3

Leonhardt, R., 2006, Analyzing rock magnetic measurements: The RockMagAnalyzer 1.0 software: Computers & Geosciences, v. 32, p. 1420–1431. doi:10.1016/j.cageo.2006.01.006

Manea, V.C., Manea, M., and Ferrari, L., 2013, A geodynamical perspective on the subduction of Cocos and Rivera plates beneath Mexico and Central America: Tectonophysics, v. 609, p. 56–81. doi:10.1016/j.tecto.2012.12.039

Morton, R.A., Gelfenbaum, G., and Jaffe, B.E., 2007, Physical criteria for distinguishing sandy tsunami and storm deposits using modern examples: Sedimentary Geology, v. 200, p. 184–207. doi:10.1016/j.sedgeo.2007.01.003

Nagata, T., 1961, Rock magnetism (second edition): Tokyo, Maruzen Company Ltd., 350 p.

Núñez-Cornú, F., Marta, L., Nava, F., Reyes-Dávila, G., and Suárez-Plascencia, C., 2002, Characteristics of seismicity in the coast and north of Jalisco Block, Mexico: Physics of the Earth and Planetary Interiors, v. 132, p. 141–155. http://dx.doi.org/10.1016/S0031-9201(02)00049-3.

Ortega, B.M., Caballero, C., Lozano, S., Israde, I., and Vilaclara, G., 2002, 52 000 years of environmental history in Zacapú basin, Michoacán, Mexico: The magnetic record: Earth and Planetary Science Letters, v. 202, p. 663–675. doi:10.1016/S0012-821X(02)00802-6

Ortiz, M., Singh, S.K., Pacheco, F.J., and Kostoglodov, V., 1998, Rupture length of the October 9, 1995 Colima-Jalisco earthquake (Mw 8) estimated from tsunami data: Geophysical Research Letters, v. 25, p. 2857–2860. doi:10.1029/98GL02059

Özdemir, Ö., and Dunlop, D., 2014, Hysteresis and coercivity of hematite: Journal of Geophysical Research: Solid Earth, v. 119, p. 2582–2594. doi:10.1002/2013JB010739

Ramírez-Herrera, M.-T., Corona, N., Lagos, M., Černý, J., Goguitchaichvili, A., Goff, J., Chagué-Goff, C., Machain, M. L., Zawadzki, A., Jacobsen, G., Carranza-Edwards, A., Lozano, S., and Blecher, L., 2014, Unearthing earthquakes and their tsunamis using multiple proxies: The 22 June 1932 event and a probable fourteenth-century predecessor on the Pacific coast of Mexico: International Geology Review, v. 56, p. 1584–1601. doi:10.1080/00206814.2014.951977

Ramírez-Herrera, M.T., Cundy, A., and Kostoglodov, V., 2005, Evidence of Prehistoric Earthquakes and Tsunamis during the last 5000 years along the Guerrero Seismic Gap, Mexico: Proceedings of the XV CNIS Mexican Society of Seismic Engineering, v. I-07, p. 1–17.

Ramírez-Herrera, M.T., Cundy, A., Kostoglodov, V., Carranza-Edwards, A., Morales, E., and Metcalfe, S., 2007, Sedimentary record of late Holocene relative sea-level change and tectonic deformation from the Guerrero Seismic Gap, Mexican Pacific Coast: The Holocene, v. 17, p. 1211–1220. doi:10.1177/0959683607085127

Ramírez-Herrera, M.T., Cundy, A., Kostoglodov, V., and Ortiz, M., 2009, Late Holocene tectonic land-level changes and tsunamis at Mitla lagoon, Guerrero, México: Geofísica Internacional, v. 48, p. 195–209.

Ramírez-Herrera, M.-T., Lagos, M., Hutchinson, I., Kostoglodov, V., Machain, M.L., Caballero, M., Goguitchaichvili, A., Aguilar, B., Chagué-Goff, C., Goff, J., Ruiz-Fernández, A.-C., Ortiz, M., Nava, H., Bautista, F., Lopez, G.I., and Quintana, P., 2012, Extreme wave deposits on the Pacific coast of Mexico: Tsunamis or storms? – A multi-proxy approach: Geomorphology, v. 139-140, p. 360–371. doi:10.1016/j.geomorph.2011.11.002

Ramírez-Herrera, M.T., and Urrutia-Fucugauchi, J., 1999, Morphotectonic zones along the coast of the Pacific continental margin, southern Mexico: Geomorphology, v. 28, p. 237–250. doi:10.1016/S0169-555X(99)00016-1

Rees, A.I., and Woodall, W.A., 1975, The magnetic fabric of some laboratory-deposited sediments: Earth and Planetary Science Letters, v. 25, p. 121–130.

Richmond, B.M., Watt, S., Buckley, M., Jaffe, B.E., Gelfenbaum, G., and Morton, R.A., 2011, Recent storm and tsunami coarse-clast deposit characteristics, southeast Hawaii: Marine Geology, v. 283, p. 79–89. doi:10.1016/j.margeo.2010.08.001

Robertson, D.J., and France, D.E., 1994, Discrimination of remanence-carrying minerals in mixtures, using isothermal remanent magnetisation acquisition curves: Physics of the Earth and Planetary Interiors, v. 82, p. 223–234. doi:10.1016/0031-9201(94)90074-4

Sanchez-Cabeza, J.A., and Ruiz-Fernández, A.C., 2012, ^{210}Pb sediment radiochronology: An integrated formulation and classification of dating models: Geochimica Et Cosmochimica Acta, v. 82, p. 183–200. doi:10.1016/j.gca.2010.12.024

Schneider, J.-L., Chagué-Goff, C., Bouchez, J.-L., Goff, J., Sugawara, D., Goto, K., Jaffe, B., and Richmond, B., 2014, Using magnetic fabric to reconstruct the dynamics of tsunami deposition on the Sendai Plain, Japan – The 2011 Tohoku-oki tsunami: Marine Geology, v. 358, p. 89–106. doi:10.1016/j.margeo.2014.06.010

Stacey, F.D., and Banerjee, S.K., 1974, The physical principles of rock magnetism, Amsterdam, Elsevier, 195 p.

Taira, A., and Scholle, P.A., 1979, Deposition of resedimented sandstone beds in the Pico Formation, Ventura Basin, California, as interpreted from magnetic fabric measurements: Geological Society of America Bulletin, v. 90, p. 952–962. doi:10.1130/0016-7606(1979)90<952:DORSBI>2.0.CO;2

Tarling, D.H., and Hrouda, F., 1993, The magnetic anisotropy of rocks, London, Champan and Hall, 217 p.

Teisseyre, A.K., 1975, Pebble fabric in braided stream deposits with examples from recent and "frozen" Carboniferous channels (Intrasdetic Basin, central Sudetes): Geologia Sudetica, v. 10, no. 1, p. 7–46.

Thompson, R., and Oldfied, F., 1986, Environmental magnetism, London, Allen and Unwin, 227 p.

Tuttle, M.P., Ruffman, A., Anderson, T., and Jeter, H., 2004, Distinguishing tsunami from storm deposits in Eastern North America: The 1929 Grand Banks Tsunami versus the 1991 Halloween Storm: Seismological Research Letters, v. 75, no.1, p. 117–131. doi:10.1785/gssrl.75.1.117

Vilas, F., Arche, A., Ferrero, M., and Isla, F., 1999, Subantarctic macrotidal flats, cheniers and beaches in San Sebastian Bay, Tierra Del Fuego, Argentina: Marine Geology, v. 160, p. 301–326. doi:10.1016/S0025-3227(99)00021-3

Wassmer, P., Schneider, J.-L., Fonfrège, A.-V., Lavigne, F., Paris, R., and Gomez, C., 2010, Use of anisotropy of magnetic susceptibility (AMS) in the study of tsunami deposits: Application to the 2004 deposits on the eastern coast of Banda Aceh, North Sumatra, Indonesia: Marine Geology, v. 275, p. 255–272. doi:10.1016/j.margeo.2010.06.007

Weiler, P.D., 2007, Magnetic anisotropy, sedimentary rocks and strain alteration, *in* Gubbins, D., and Herrero-Bervera, E., eds., Encyclopedia of geomagnetism and paleomagnetism, Dordrecht, Springer, p. 475–477.

Williams, P.E., and Rust, B.R., 1969, The sedimentology of a braided river: Journal of Sedimentary Petrology, v. 39, no. 2, p. 649–679.

Yagishita, K., 1997, Paleocurrent and fabric analyses of fluvial conglomerates of the Paleogene Noda Group, northeast Japan: Sedimentary Geology, v. 109, no. 1–2, p. 53–71. doi:10.1016/S0037-0738(96)00058-9

Zeeden, C., Hambach, U., and Händel, M., 2015, Loess magnetic fabric of the Krems-Wachtberg archaeological site, Quaternary International, v. 372, p. 188–194.

Zhou, W., Van Der Voo, R., Peacor, D.R., and Zhang, Y., 2000, Variable Ti-content and grain size of titanomagnetite as a function of cooling rate in very young MORB: Earth and Planetary Science Letters, v. 179, p. 9–20. doi:10.1016/S0012-821X(00)00100-X